Journal of Structural Geology, Vol. 11, No. 5, pp. 539 to 551, 1989
Printed in Great Britain

0191-8141/89 $03.00 + 0.00

Strain history of the Los Prietos syncline, Santa Maria basin, California: a case of post-tectonic compaction

RICHARD T. CHEN and GERHARD OERTEL

Department of Earth and Space Sciences, University of California, Los Angeles, CA 90024, U.S.A.

(*Received* 10 *September* 1987; *accepted in revised form* 19 *December* 1988)

Abstract—Strain measurements of the Monterey Shale along a fold profile of the Los Prietos syncline in the Santa Maria basin, California, provide an opportunity to study the strain history of the syncline. By using transmitted X-ray goniometry, we first measured the degree of preferred orientation of chlorites in 19 samples along the profile. From the preferred orientations, total strains were calculated according to March's theory. Based on the variation of the total strains along the asymmetrical syncline, a plausible history could have been as follows: compaction first reduced the porosity from 86 to 79%; before beds were fully consolidated, they were buckled and then homogeneously strained, on the average, by strains of [1.00, −0.27, −0.32] with a nominal standard deviation of 0.01. The rheology during deformation of the unconsolidated rocks made the folding style resemble one of soft-sediment deformation. Finally, the porosity was further reduced by a post-tectonic vertical compaction to 40% of the original pore volume.

The deformation history of the syncline appears to be related to the development of the pull-apart Santa Maria basin. The relationship between the geometry of the syncline and the orientation of the principal axes of the homogeneous tectonic strain are consistent with a tectonic strain history in three increments, basin opening, folding and westward tilting.

INTRODUCTION

BASED on March theory (1932), strain in deformed rocks has been successfully determined from the preferred orientation of phyllosilicates (Means & Paterson 1966, Oertel 1970, Tullis 1971, 1976, Oertel & Curtis 1972, Oertel 1974, Tullis & Wood 1975, Oertel & Ernst 1978). The measured strain is the total strain accumulated throughout the history of deformation (Etheridge & Oertel 1979, Oertel 1983). It includes non-tectonic strains, such as those due to compaction, slumping or bioturbation, together with tectonic strains. By collecting samples in a region with contrasting strains (Krishnan & Oertel 1980), or in a concretion which recorded strain history during its growth (Oertel & Curtis 1972), one may separate the tectonic from the non-tectonic strains.

Sediments deposited in a tectonically active basin could hypothetically be subjected to an interplay of tectonic strain and compaction, and this could happen before the sediments are consolidated. The ductility of water-rich sediments will be reduced with the progress of consolidation (Maltman 1984). The result could be a deformational style that combines features of brittle deformation and ductile deformation. The deformational style alone, however, is not sufficient to indicate the cause of deformation (Elliott & Williams 1988). A possible example of gradually consolidated sediments is the Miocene Monterey Formation deposited in several of the basins that opened during the late Cenozoic in the Californian continental borderland (Crowell 1974). The intriguing style of folding in these rocks has been studied by Johnson & Page (1976), Snyder *et al.* (1983) and Snyder (1987). Intraformational folds are more common and vary more in shape in the Monterey Formation than in formations nearby with the same degree of overall deformation. Snyder (1987) suggested that these structures commonly combine syndepositional folding with later tectonic folding. Johnson & Page (1976) studied the development of intraformational concentric-like and chevron-like folds and the possible mechanisms of their formation in the Huasna syncline. They concluded that layer-parallel slip is the primary folding mechanism; the folds form and their dimensions are controlled in response to the stress, the rheological properties of the rocks at the time of folding, and the thickness of the layers. The location of intraformational folds within first-order folds affects their shapes. Snyder *et al.* (1983) and Brueckner *et al.* (1987) pointed out that the structural style is also determined by the timing of tectonic events and by the state of diagenesis of siliceous sediments during deformation, insofar as water content and diagenesis affect the rheological properties. However, the potential effect of an episode of post-tectonic compaction on fold shapes in the Monterey Formation has not, so far, been studied because quantitative strain determinations are needed for such an attempt.

This study examines parasitic folds in an asymmetric syncline in the Monterey Formation, estimates the strains at various points along the fold profile by measuring phyllosilicate preferred orientation, attempts to separate the tectonic from the non-tectonic strains, and derives a model to explain the strain history.

REGIONAL SETTING

The Los Prietos syncline (Dibblee 1966) forms part of the eastern tip of the Santa Maria basin. The basin, a wedge-shaped pull-apart basin (Fig. 1) (Hall 1978, 1981, fig. 17-2), is bounded on the north and northeast by the

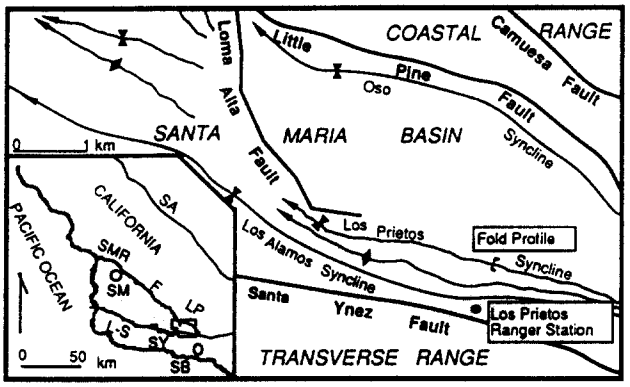

Fig. 1. Generalized fold and fault map of the eastern Santa Maria basin, modified from geologic map of the Goleta and San Rafael Mtn, 15-minute Quadrangles, Santa Barbara County, California (Dibblee 1966). The study area is in the eastern third of the map. Traces of anticlinal culminations (light lines with divergent arrows), synclinal troughs (light lines with convergent arrows), and faults (heavy lines) are shown.
Insert map modified from fault map of West Central California (Hall 1981, fig. 17-2). It shows the major faults near the Santa Maria basin (dotted) and the location of the main map (box). Faults: F, Foxen; LP, Little Pine; L–S, Lompoc–Solvang; SA, San Andreas; SMR, Santa Maria River; SY, Santa Ynez. Towns: SB, Santa Barbara; SM, Santa Maria.

Little Pine–Foxen Canyon–Santa Maria River fault system, and on its south and southwest by the Lompoc–Solvang and part of the Santa Ynez fault systems; furthermore, its west side was truncated by right-lateral slip on the San Simeon–Hosgri fault after the basin was formed. The Coast Ranges lie north of the basin, the Western Transverse Range south of it.

According to a paleomagnetic reconstruction of southern California (Luyendyk *et al.* 1980, Hornafius 1985, Hornafius *et al.* 1986, Luyendyk & Hornafius 1987) the Santa Maria basin has evolved between rotating microplates. During Middle Miocene (15–10 Ma b.p.), the originally N–S-oriented Santa Ynez Range rotated 50° clockwise about its southern (now western) end, causing crustal extension and basement subsidence in the basin (see fig. 11 in Hornafius 1985). After a pause (from 10 to 5 Ma b.p.), a further 30° rotation of this range, but now about its eastern end (see fig. 12 in Hornafius 1985), produced the Plio-Pleistocene tectonic shortening and uplift inside the basin described by Woodring & Bramlette (1950). Judging from the fold trends in the basin, the overall direction of shortening was between N–S and NE–SW. That folds and faults converge toward the acute-angled eastern basin tip and that uplift is strongest in the same corner suggest that shortening was more intense at the eastern end of the basin.

The Monterey Formation was deposited at the height of basin opening (late Mid-Miocene to late Miocene); the sea flooded the whole basin. The thickness of the Monterey Formation varies from basin rim to center from 1100 to 630 m (Hall 1978). Most of the Monterey rocks were deposited as a deep marine facies (Ingle 1980). Pisciotto & Garrison (1981) subdivided them into a lower calcareous, a middle phosphatic transitional and an upper siliceous facies. All three subfacies of the Monterey Formation occur in the Santa Maria basin, but generally the siliceous facies is the predominant one.

DIAGENESIS AND RHEOLOGY

Monterey Formation silica undergoes a three-stage diagenetic transformation from opal-A to opal-CT to quartz (Murata & Larson 1975). The degree of silica diagenesis is governed by depth of burial, temperature and by the amount of detrital material intermixed with the silica. In general, the more deeply buried rocks reached higher temperatures and have a higher degree of diagenesis. The higher the content of detrital grains in the rock, the higher is the transformation temperature from opal-A to opal-CT, but the lower is the transformation temperature from opal-CT to quartz. Generally, porosity decreases and density, hardness, cohesion and brittleness increase with the progression of silica diagenesis, most drastically with the transitions to opal-CT and to quartz. Because of rhythmic alternations of beds with different detrital grain contents, up to three different stages of diagenetic alteration coexist commonly in neighboring layers (Isaacs *et al.* 1983).

Dolomitization is another diagenetic process which can strongly affect the rheology of Monterey rocks. Where it occurs, either as discrete layers or as giant nodules, it markedly enhances brittleness. Fracturing and brecciation commonly followed the dolomitization. In places, dolomite was formed in several cycles, each new wave being superposed on the older. Therefore, products of a later dolomitization cycle can re-cement breccia units that have been broken by being subjected to stress after embrittlement by the previous cycle; after such re-cementation, renewed fracturing may brecciate the rocks once again (Redwine 1981, Roehl 1981). The dolomitization does not preferentially affect rocks in the vicinity of faults or folds, and the factors which control the process are unknown.

Compaction by the weight of overlying younger sediments tends to close the pores between detrital grains and to increase rock competency. Isaacs (1981), in her study of the Monterey Formation along the Santa Barbara coast, concluded that disseminated secondary dolomite reduced porosity by less than 10%. One may, therefore, use porosity reduction as a fairly reliable indicator of the degree of compaction in the Monterey Formation. A general pattern of porosity reduction related to burial depth and progress of silica diagenesis in diatomaceous rocks was shown to exist by Isaacs *et al.* (1983); their fig. 8(a) is here reproduced as Fig. 2. An initial sediment porosity of 86%, adopted by Isaacs *et al.* and here, was originally cited by Hamilton (1976) who took it from measurements in the upper 30 cm of a core from a recent deposit of diatomaceous ooze in the Bering Sea. Isaacs *et al.* (1983) indicated, in addition to a gradual compaction, two abrupt steps of porosity reduction that are directly related to the two silica phase transformations. The pore framework, originally supported by diatom frustules or opal-CT, is weakened

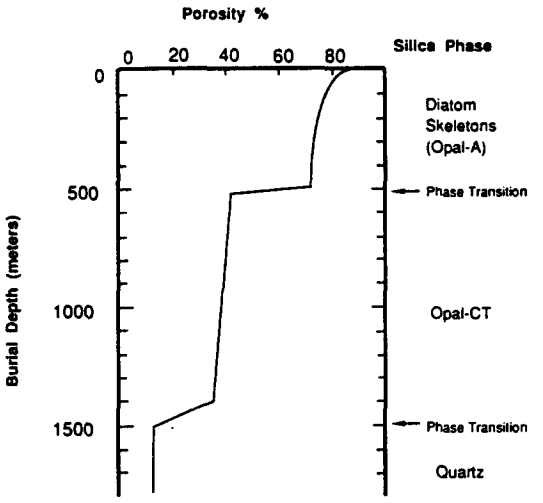

Fig. 2. Porosity as a function of depth of burial in diatomaceous rocks (after Isaacs *et al.* 1983, fig. 8a). Porosity changes with depth in the manner of a step function, the steps corresponding to the two silica phase transitions.

by rearrangement of silica during the two phase transformations. With each transformation, grains were pushed closer together. This reduces porosity from approximately 70 to 40% during the transition from opal-A to opal-CT, and from approximately 35 to 10% during the transition from opal-CT to quartz.

DESCRIPTION OF FOLD PROFILE

The Los Prietos syncline is exposed on a north-bank cliff cut by the Santa Ynez River between the Oso and Aliso Canyons. The cliff is about 120 m high, well exposed and uninterrupted by major faults for about 90 m along the river. The horizontal trace of the profile trends approximately 020°. The whole outcrop was mapped as Upper Monterey Formation by Dibblee (1966). Exposed along the cliff are diatom-rich rocks of the siliceous facies, diagenetically in the opal-CT state, irregularly alternating with diatom-poor opal-CT mudstones containing disseminated dolomite nodules. Like most Upper Monterey Formation elsewhere, these rocks show alternations of laminated and massive layers.

The fold is an asymmetrical syncline (see axial profile in Fig. 3b) with its near-vertical NE limb about one third thinner than its gently northward-dipping SW limb. The fold axis trends 311° and plunges 22°NW. The gently dipping limb has an average strike of 093° and a dip of 26°N and the steep limb a strike of 134° and dip of 73°SW. Near the hinge area, beds strike on average 172° and dip 37°W. Faults truncate both ends of the profile section. The fold tightens toward its core, and in the innermost core exposed on the cliff the north limb is overturned. However, at higher levels in the syncline than those exposed in the profile, younger rocks, as shown in the geological map (Dibblee 1966), are folded less tightly. This may indicate that folding of the Monterey rocks in this syncline could have started before all of its enclosed sediments were deposited.

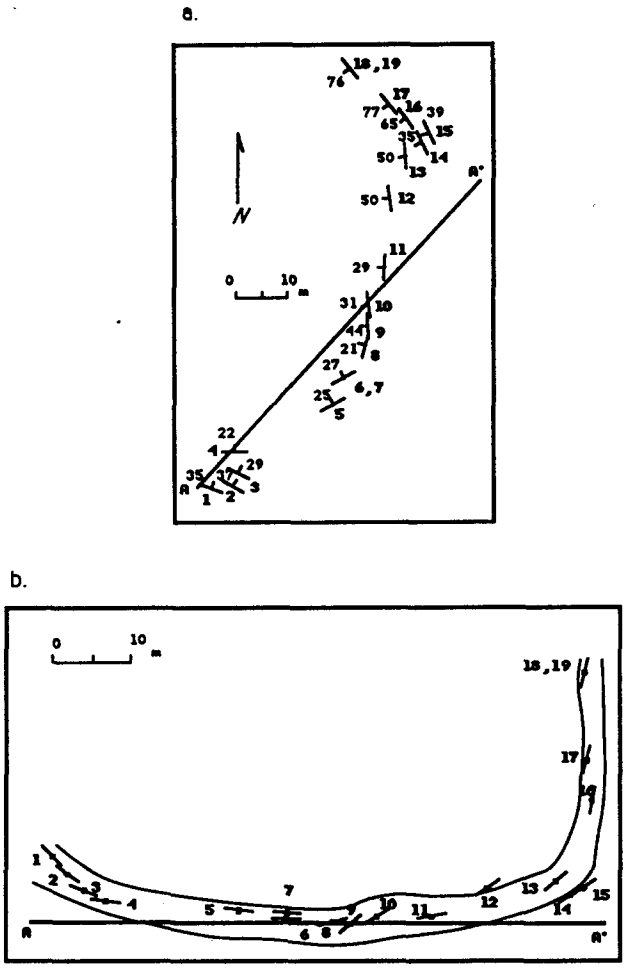

Fig. 3. (a) Sample map to show locations of sample points and bedding attitudes: faint numerals—strikes, bold numerals—sample numbers; A–A', N44°E strike line of profile plane (normal to fold axis). (b) Axial profile; short bars show the apparent dip.

A variety of minor structures affecting bedding can be observed across the profile. Generally, each kind is confined to a stratigraphic thickness of less than 5 m. They may be divided into features presumably due to a history of extension (thinning) or of shortening (thickening) parallel to the bedding plane, or of a mixture of the two. For brevity, we will call those features 'extensional', 'contractional', or 'mixed-origin'.

The extensional features are local, curved, normal faults (Fig. 4a), and dip-accentuating small-scale monoclines with a thinned steep limb (Fig. 4b). Where a normal fault (subarea 1 in Fig. 4a) has its top termination, there is an extensional depression filled by material from a relatively ductile layer. The displacement along the fault is accommodated by internal deformation of this layer; overlying beds are unaffected by the fault. Layers cut by the fault show drag folds near the fault (subarea 2 in Fig. 4a). At its bottom termination (subarea 3 in Fig. 4a), the normal fault swerves into parallelism with bedding and thus changes into a bedding-plane fault within a ductile layer. Some layers are missing on the hangingwall. Development of the small-scale monocline (Fig. 4b) could have preceded the initiation of a curved normal fault (Fig. 4a). Layer

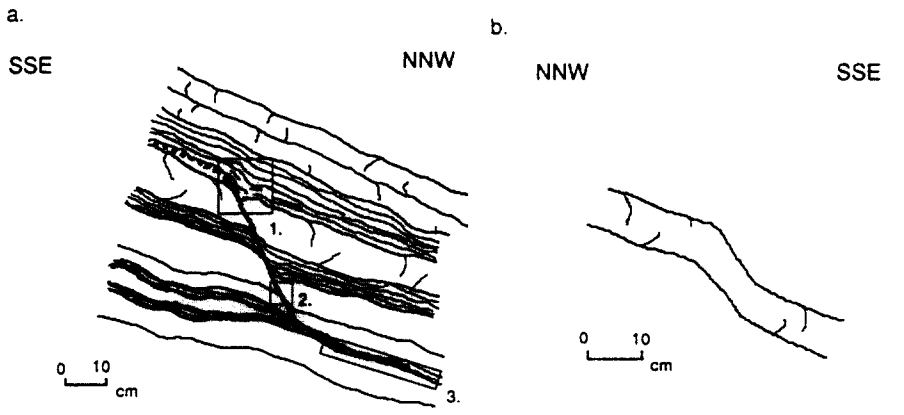

Fig. 4. Profile views of extensional small-scale structures. (a) Curved normal fault between sample points 1 and 2. Subarea 1: tensional depression filled by ductile material. Subarea 2: 'drag fold'. Subarea 3: transition from normal fault to bedding plane fault. (b) Dip-accentuating small-scale monocline near sample point 4. The sample localities are shown in Fig. 3.

continuity may have been disrupted in the thinned portion as faulting occurred. Truncation of the inclined portion of the micromonocline could then have produced the appearance of drag folds against the fault.

Contractional small-scale structures are microfolds and associated reverse microfaults (Figs. 5a–c). Locally, a stack of beds may show a bulge caused by compressional thickening combined with kink folding of the constituent beds (Fig. 5a). Ductile layers are most thickened in kink fold hinges. Reverse microfaults occur most commonly in the straight limbs between hinges of kink folds (Fig. 5b, fault a). Some reverse faults form large angles with the layers they truncate (subarea 1 in Fig. 5c). Like normal faults, small-scale reverse faults can have transitions into bedding plane faults (subareas 2 and 3 in Fig. 5c). Hangingwall rocks are wedged upward underneath the continuous layers to produce in the latter an asymmetric upward bulge. Similarly, in the footwall the underlying continuous layers bulge downward asymmetrically. Figures 5(a)–(c) show observed features that could have been successive stages of the evolution of a contractional feature. At an early stage of shortening parallel to the bedding, kink folds may have occurred within a stack of beds (Fig. 5a). Then, reverse microfaults truncated the folded beds in the straight limbs between hinges of the kink folds (Fig. 5b). Finally, one of the microfaults (Fig. 5c) propagated outward into bedding planes of the undisturbed stack.

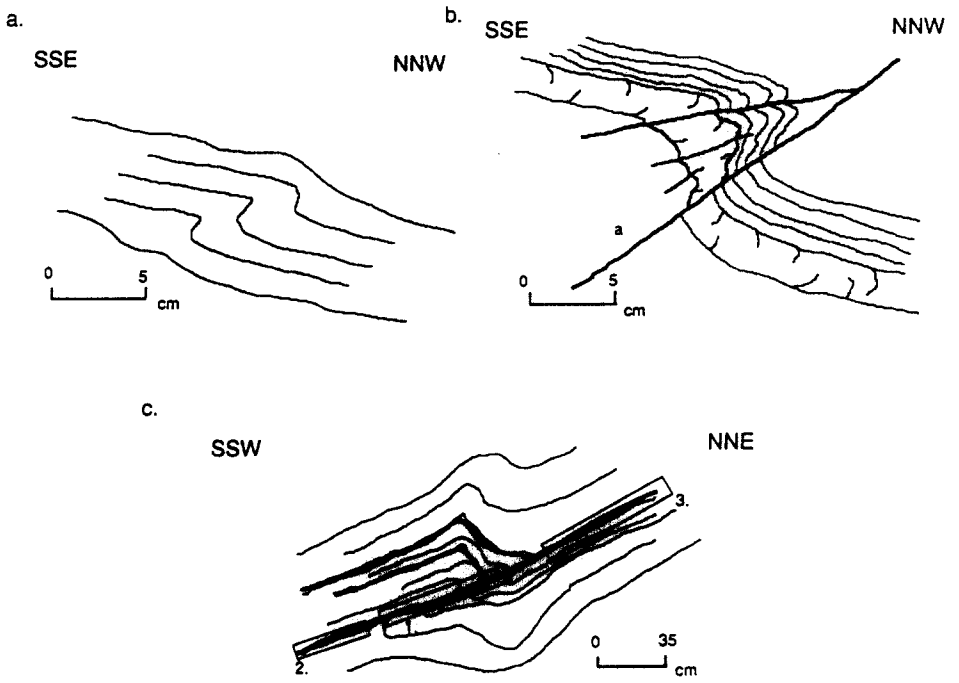

Fig. 5. Profile views of contractional small-scale structures. (a) Kink fold near sample point 1. (b) Reverse microfaults associated with a fold, near sample point 1. (c) Reverse microfault with transition to bedding-plane fault and associated with folds about 10 m northeast of sample point 15. Subarea 1: layers truncated by the reverse microfault. Subareas 2, 3: the microfault has become a bedding-plane fault. Sample localities are shown in Fig. 3.

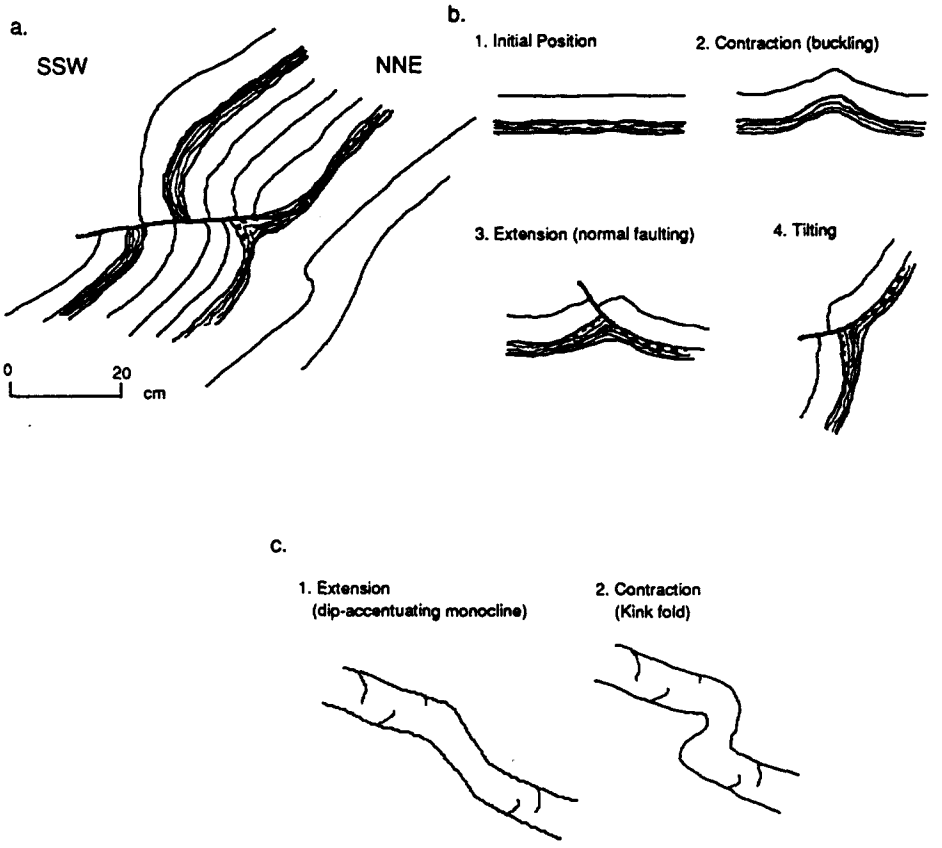

Fig. 6. Mixed-origin small-scale structures. (a) Extensional overprint on a fold 15 m northeast of sample point 15 in Fig. 3. (b) Sketches of a hypothetical history of the structure in (a). (c) Contraction overprint on a small-scale monocline, an alternative development history of kink folds as in Fig. 5(a).

The third category of small-scale structures has mixed attributes and could have been due to extensional structures overprinting earlier contractional ones (Fig. 6a) or vice versa (Fig. 6c). The structure of Fig. 6(a) was observed in the steep north limb of the major syncline. Hypothetical sketches of the most plausible history of this structure are shown as Fig. 6(b). A pair of beds, competent above incompetent (1 in Fig. 6b), was first buckled (contractional) (2 in Fig. 6b), then normally faulted (extensional) (3 in Fig. 6b), and finally rigidly tilted (4 in Fig. 6b). A hypothetical contractional structure overprinting an earlier extensional one is shown in Fig. 6(c). A small-scale monocline is assumed to have been formed first, followed by kinking. This is a possible alternative history for the development of the kink folds shown in Fig. 5(a).

All the described small-scale structures were found at the same stratigraphic level over a thickness of less than 25 m. Thus, thinning and thickening interplayed within the same packet of beds. The axes of all the small-scale folds in this packet deviate little in attitude from the axis of the syncline as a whole (Chen 1986). This indicates that the small folds are probably parasitic to the large one and are genetically related to it.

Intraformational structures like those described above are commonly observed throughout the Monterey Formation. They were described by previous investigators as soft-sediment deformation structures resulting from passive gravitational slope failures (Bramlette 1946, Redwine 1981, Snyder 1987). Since the microstructures in this study are systematically related to tectonically caused folding, but have a deformational style that resembles one caused by soft-sediment deformation, they could have resulted from tectonic events which unevenly depressed or uplifted the basement, triggering slope failure before the sediments were fully consolidated.

Nineteen samples were collected along the profile of the syncline (Fig. 3) at a particular stratigraphic level (within a 5 m thickness) and analyzed for the preferred orientation of phyllosilicates and for the March strain. Sample Nos 1–7 are from the south limb, Nos 8–15 from the hinge area, and Nos 16–19 from the north limb. To eliminate local inhomogeneities of the strain field as much as possible and to be able to compare strains in rocks of similar rheology throughout the profile, dolomite nodules and the matrix in their vicinity, and regions disturbed by small-scale structures were not sampled. For the same reasons, all sections for X-ray study were cut from the massive portions of samples that show an alternation between laminated and massive beds.

STRAIN DETERMINATION

March's (1932) method was applied to estimate strain in the 19 samples. The estimates are subject to some of the reservations expressed by Etheridge & Oertel (1979)

Table 1. Principal stretches and their directions, s_1: maximum, s_2: intermediate, s_3: least

Sample No.	s_1	Trend (°)	Plunge (°)	s_2	Trend (°)	Plunge (°)	s_3	Trend (°)	Plunge (°)
LP-01	1.20	351	34	1.16	92	16	0.72	201	52
LP-02	1.17	29	42	1.17	296	4	0.72	202	47
LP-03	1.20	4	29	1.15	96	5	0.73	196	62
LP-04	1.13	351	17	1.12	259	7	0.78	147	71
LP-05	1.22	312	31	1.19	47	9	0.69	151	58
LP-06	1.13	273	23	1.11	16	27	0.80	148	53
LP-07	1.22	32	25	1.11	283	37	0.69	147	44
LP-08	1.24	329	10	1.06	237	15	0.76	91	71
LP-09	1.16	337	20	1.08	234	34	0.79	94	51
LP-10	1.21	340	12	1.17	243	28	0.70	91	59
LP-11	1.23	304	32	1.20	210	5	0.68	110	60
LP-12	1.13	358	6	1.12	255	49	0.79	87	40
LP-13	1.12	189	16	1.05	292	39	0.85	81	48
LP-14	1.11	339	3	1.09	247	37	0.83	73	52
LP-15	1.17	334	11	1.09	237	31	0.79	81	57
LP-16	1.13	161	32	1.05	286	42	0.84	49	31
LP-17	1.13	153	21	1.09	290	62	0.81	57	18
LP-18	1.08	129	23	1.07	279	63	0.85	34	12
LP-19	1.15	144	47	1.07	296	40	0.81	39	14

and Oertel (1983). The degree of preferred orientation of platy strain marker grains was measured on an X-ray pole figure goniometer in the transmission mode. The method has been described by Baker *et al.* (1969), Oertel (1970), Wood *et al.* (1976) and Wenk (1985). In the present study, chlorite grains were chosen as strain markers, because their measurement yielded the highest signal-to-background ratio.

March (1932) formulated the equation,

$$\varepsilon_i = \rho_i^{-1/3} - 1, \qquad (1)$$

where ε_i is a principal strain at constant volume, defined as a ratio of length change of a material line to its original length, and ρ_i is the normalized frequency of poles of the basal planes of the strain markers in one of the principal directions. March considered the geometry of passive markers, originally oriented at random, and allowed to deform homogeneously within a matrix taken to have experienced no volume change. To apply his model, one must make the untested assumption that the only mechanism by which markers respond to the deformation is passive rotation; other possible mechanisms of preferred orientation such as intracrystalline deformation, recrystallization or preferred crystallization (Etheridge & Oertel 1979) must be excluded. Because the X-ray pole figures for the 19 samples generally have nearly orthorhombic symmetry, it is reasonable to assume that the deformation is homogeneous at the scale of each sample. As to the assumption of an original random orientation distribution of the markers, clay mineral grains have been shown to settle on the ocean floor as pellets or as flocculated aggregates without preferred orientation (Meade 1966, Blatt *et al.* 1980, p. 121). Preferred orientation of clay-sized particles is developed by subsequent compaction (Faas & Crocket 1983, Moon & Hurst 1984). Therefore, the strains in the Monterey Formation estimated by the March method are cumulative strains from the moment the sediments were first deposited.

The estimated principal total stretches $(1 + \varepsilon_i)$ and their directions for 19 samples are listed in Table 1. They range from 0.68 to 0.85 for the least stretch, from 1.05 to 1.20 for the intermediate and from 1.08 to 1.24 for the maximum stretch. The mean principal total stretches of all 19 samples and of the subpopulations from the three sections of the fold (north limb, hinge and south limb, Table 2) were calculated by the following steps. First, convert principal March strains to natural strains, then express these in geographic reference co-ordinates (north, east and down). Second, take the arithmetic average for each component over the 19 samples for an overall mean and also over the four samples from the north limb, the eight from the hinge and the seven from the south limb for three subpopulation means. Finally, find for each set of averaged components the directions and values of the principal strains and convert the values to principal stretches. As a measure of the dispersion, the average estimated standard deviations of the means

Table 2. Mean principal stretches and their directions in the north limb, hinge area, south limb and overall; s_1: maximum, s_2: intermediate, s_3: least

	s_1	Trend (°)	Plunge (°)	s_2	Trend (°)	Plunge (°)	s_3	Trend (°)	Plunge (°)
North limb	1.11	149	37	1.07	294	46	0.84	45	18
Hinge area	1.16	334	12	1.10	241	31	0.78	88	56
South limb	1.16	357	32	1.13	263	1	0.76	172	57
Overall	1.14	318	24	1.03	224	9	0.86	116	63

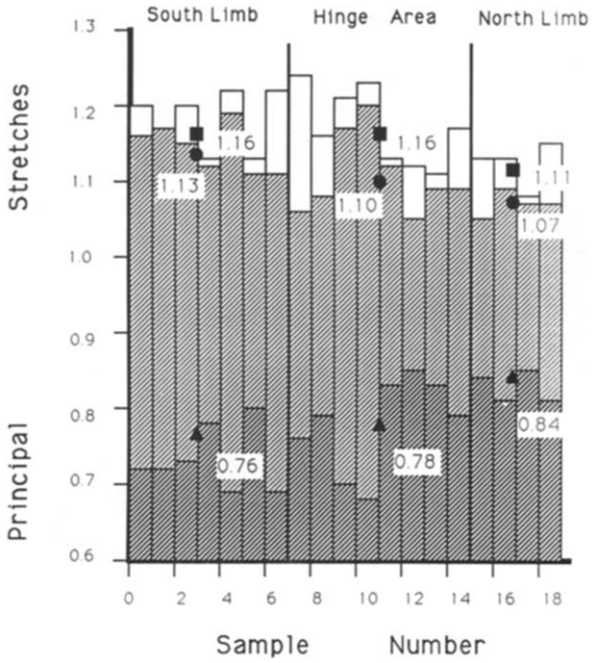

Fig. 7. Variation of principal stretches along the fold profile: heavy shaded bars—least principal values; light shaded bars—intermediate principal values; unshaded bars—maximum principal values; black—means of each subpopulation. (Square—maximum; circle—intermediate; triangle—minimum.) Numbers indicate the mean principal values of subpopulations.

of the nine components of natural strains in the geographic co-ordinates were calculated. They are 0.09 for the overall mean, 0.03 for the north limb, 0.05 for the hinge and 0.07 for the south limb. Figure 7 shows the variation of principal values sample by sample and the mean principal values in the three sections of the fold. Figures 8(a)–(c) are synoptic equal-area projections showing principal directions for the three subpopulations and their means, and Fig. 8(d) shows overall mean principal directions. The measured least principal stretches generally increase from the south to the north limb (Fig. 7), and the principal directions are increasingly scattered in the reverse order (Figs. 8a–c). The overall mean principal stretches are [1.14, 1.03, 0.86] with an average standard deviation of 0.09. The mean maximum is nearly parallel to the fold axis, the mean intermediate axis is nearly horizontal and normal to the fold axis, and the mean least axis plunges steeply (Fig. 8d).

FACTORIZATION OF STRAINS

The strain data show that the gently dipping south limb, in contrast to the conventional model of compaction followed by folding, has more shortening normal to

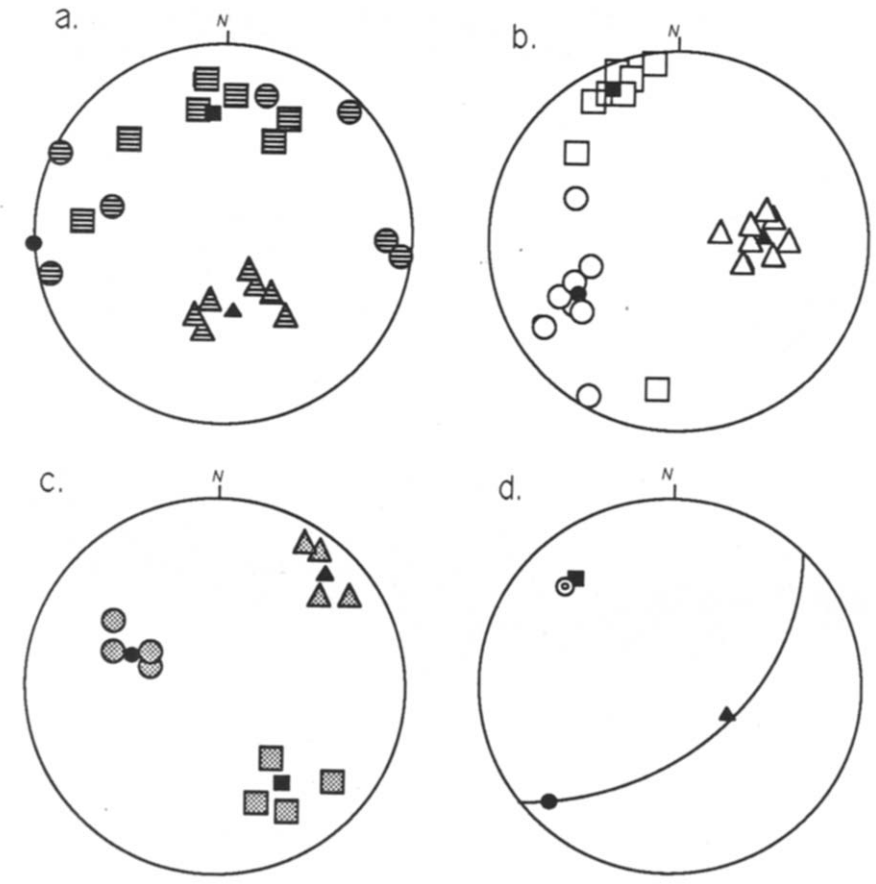

Fig. 8. Synoptic equal-area projections of principal strain directions: (a) south limb; (b) hinge area; (c) north limb; (d) overall mean. Squares—maximum, circles—intermediate, triangles—least principal strain directions. Ruled—south limb. Open—hinge area. Dotted—north limb. Black—means of each subpopulation in (a–c), mean of overall in (d). Double circle—fold axis. Great circle—normal to fold axis.

the bedding than has the steeper north limb (Fig. 7, and Tables 1 and 2). To explain this excess thinning of the gently dipping beds, additional compaction must be postulated, which had to occur after the several portions of the fold had been rotated to approximately their present position. A potential strain history was derived by trying various sequences of separate strain events, using a trial and error method, to find a sequence that is relatively simple, plausible and the results of which approximately agree with observations. From this procedure, the sequence of straining events may have been as follows. First, the Monterey sediments were deposited with an initial porosity of 86%. Pre-tectonic compaction reduced porosity to a certain value that will be called the pre-tectonic porosity from here on. Buckling then rotated the beds approximately to the present position, and after that followed a phase of homogeneous tectonic straining. Finally, post-tectonic compaction followed the tectonic events and reduced the porosity to 40%, the upper limit for opal-CT bearing rocks in Isaacs *et al.*'s (1983) study. For simplicity, in the following calculation, the 19 strain measurements were divided into the same three groups, corresponding to the north limb, hinge area and the south limb, that were used previously. For lack of a larger data base, the pre- and post-tectonic compaction, and the tectonic strain were assumed to have been homogeneous at the scale of the fold profile, and buckling was considered to consist of simple rigid-body rotations, separate for each of the fold sections. Each straining event was treated as a finite strain assumed to occur sequentially and to produce a cumulative total strain.

Ideally, the strain sequence could be described by the following matrix equations which are, in geographic reference co-ordinates:

$$S_i^* = C_{ps}^* T^* [A^*{}_i C_{pr}^* A_i^{*T}], \tag{2}$$

where

- i ranges from 1 to 3 and represents the sections of north limb, hinge area and south limb;
- S_i^* is an ideal total stretch tensor for section i of the fold;
- C_{ps}^* and C_{pr}^* are ideal post- and pre-tectonic compaction stretch tensors;
- T^* is an ideal homogeneous tectonic stretch tensor; and
- A_i^* is an ideal rotation matrix that rotates section i of the fold to the post-buckling position.

The tectonic stretch tensor, T^*, can be found by multiplying by inverses of C_{ps}^* and $[A_i^* C_{pr}^* A_i^{*T}]$ on both sides of equation set (2) as follows

$$T^* = C_{ps}^{*-1} S_i^* [A_i^* C_{pr}^* A_i^{*T}]^{-1}. \tag{3}$$

In the absence of evidence for rapid fluid escape from the rock, the desired homogeneous tectonic stretch, T^*, is assumed to represent a strain at constant volume. All the pore water loss is attributed to a protracted compaction process. For simplicity and for lack of constraints however, we treat the tectonic stretch as a single event, although it is known from the stratigraphic record to have consisted of at least two episodes, a first during the opening, a second during the shortening of Santa Maria basin. Because the tectonic strain is taken to have been homogeneous throughout the fold, one single tensor T^* should be found for the three different combinations of S_i^* and A_i^*.

To find the tectonic stretch tensor from the observed March strains, from guessed compaction tensors and from approximated rigid-body rotation matrices, equations (3) are modified as follows:

$$[T_i R_i] = C_{ps}^{-1}(x)[V_{ps}(x) S_i V_{pr}(x)][A_i C_{pr}(x) A_i^T]^{-1}, \tag{4}$$

where

- $[T_i R_i]$ is a transformation matrix, a matrix product of a tectonic stretch tensor, T_i, by a rotation matrix, R_i, for section i of the fold;
- x is the pre-tectonic porosity, a variable;
- $C_{ps}^{-1}(x)$ is the inverse post-tectonic compaction stretch tensor, a function of x;
- $C_{pr}(x)$ is the pre-tectonic compaction stretch tensor, a function of x;
- $V_{ps}(x)$ is a volume-compensatory matrix for the volume reduction by post-tectonic compaction, a function of x;
- $V_{pr}(x)$ is a volume-compensatory matrix for the volume reduction by pre-tectonic compaction, a function of x;
- S_i is the observed mean March stretch tensor for section i of the fold; and
- A_i is the approximate rotation matrix that rotates section i of the fold to the present position.

Assuming both the pre- and the post-tectonic compaction to have acted in a tectonically quiescent basin that did not change its horizontal dimensions, we take both to have been strictly uniaxial strains, negative vertically and not affecting horizontal lengths. As previously discussed, porosity loss was used as the indicator for total compaction. The relationship between vertical compaction strain C_v and porosity, according to Oertel & Curtis (1972), is:

$$C_v = \frac{P_o - P}{P - 100}, \tag{5}$$

where P_o and P are the initial and final porosities in per cent. The compaction stretch tensor C_{ij} then takes the form

$$[C_{ij}] = \begin{bmatrix} 1 & 0 & 0 \\ 0 & 1 & 0 \\ 0 & 0 & C_v + 1 \end{bmatrix}. \tag{6}$$

In this study, for the pre-tectonic compaction, the initial porosity, P_o, was taken to be 86% and the final porosity, P or a pre-tectonic porosity x, was treated as a variable; for the post-tectonic compaction, P_o was set $P_o = x$, and P was taken to be 40%. Therefore, both compaction tensors, $C_{ps}(x)$ and $C_{pr}(x)$, are functions of the pre-tectonic porosity x. The unknown variable x also shows

at which stage of the compaction history the tectonic event must have occurred. By assigning a value between 40 and 86% to x, $C_{pr}(x)$, $C_{ps}(x)$, and thus $C_{ps}^{-1}(x)$ are determined.

Because March strain is expressed as a nominal constant-volume strain, to compensate for the volume reduction during the two compaction events, two volume-compensatory matrices, $V_{ps}(x)$ and $V_{pr}(x)$, were applied to each mean March stretch tensor, S_i, in equation (4). They are isotropic matrices with three identical diagonal components that are the reciprocal cubic roots of the determinants of their corresponding compaction stretch tensors. These compensatory matrices are thus also functions of x.

A_i^* in equations (3), the rigid-body rotation matrices, account for the tectonic buckling which rotated the beds from the original horizontal position to an only approximately known post-buckling orientation. In the present study, it is taken to have preceded the homogeneous tectonic straining event. Since the exact post-buckling orientations are not observable, the present bedding orientations were used instead. The approximate rotation matrices, A_i in equations (4), for each section of the fold were obtained in two steps. First, horizontal beds were rotated, about a common horizontal axis trending 311°, by 73° and 29° clockwise and 22° counterclockwise for north limb, hinge and south limb, respectively. Then they were rotated 12°, 26° and 18° clockwise to their present positions about a common second horizontal axis normal to the fold axis. The resulting matrices A_i are shown in Table 3.

Three different transformation matrices, $[T_iR_i]$, which contain the tectonic stretch tensor, T_i, and a rotation matrix, R_i, can be derived from equations (4) by assigning a pre-tectonic porosity x and using A_i instead of A_i^*. The rotation matrix R_i is separated from each $[T_iR_i]$ by left polar decomposition (rotation assumed as preceding the tectonic strain). To conform with the assumption of homogeneous straining, a suitable value of x should yield three approximately equal tensors close to the ideal homogeneous tectonic stretch tensor T^* and a suitable choice of A_i should result in R_i representing negligible rotations. On this basis, a trial and error set of solutions can be attempted with the goal of converging on the most suitable solution. The components of the S_i matrices inserted into equations (4) are listed in Table 4.

The variations of both the principal values (Fig. 9) and orientations (Fig. 10) of the three calculated tectonic tensors, T_i, as functions of x were examined by arbitrarily assigning to x the four values, 50% (equivalent to no post-tectonic compaction), 60, 70 and 80% (equivalent

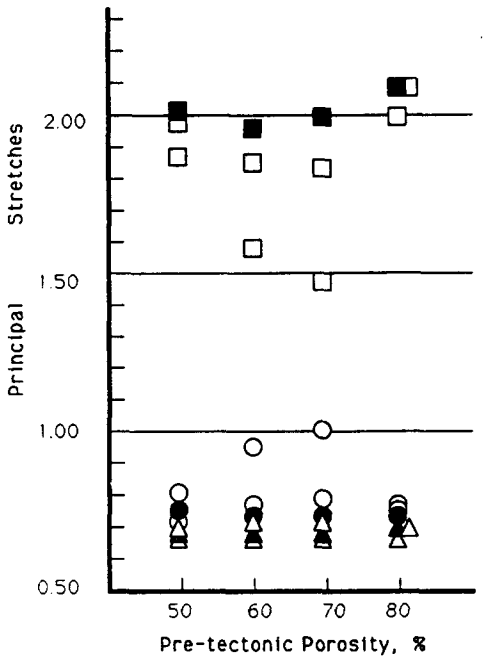

Fig. 9. Relationship between assumed pre-tectonic porosity, x, and calculated principal tectonic stretches, T_i, in the three sections of the fold. Symbols as in Fig. 8.

to syndepositional tectonic deformation). Changes of x have more effect on the orientations than on the principal values. The maximum axes from the three sections of the fold converge toward a near-vertical direction, the intermediate axes converge to a near-horizontal and NE–SW direction, and the least axes converge to a near-horizontal and NW–SE direction, as x is changed systematically from 50% to 60% to 70%. However, when x is increased to 80%, the various principal directions pass the points of convergence and they begin to diverge again dramatically. The differences between corresponding principal values increase with x increasing from 50 to 70%, then decrease as x further increases to 80%. The optimal value of x is at 79%, where both principal values and orientations of the tectonic stretches for the three parts of the fold are most nearly homogeneous (Fig. 10 and Table 5). The rotation matrices R_i at the optimal value of x are shown in Table 6; all their rotation angles are less than 1.5°. This suggests that the post-buckling orientations of the bedding did not differ much from the present orientations, which were used for the calculations as approximate final bedding orientations after buckling. The overall mean principal tectonic stretches are [2.00, 0.73, 0.68] with an average standard deviation of 0.01; the maximum stretching axis points up (Fig. 10), and the horizontal

Table 3. Approximate rotation matrices moving beds from original horizontal position to the observed orientations (see text)

	a_{11}	a_{12}	a_{13}	a_{21}	a_{22}	a_{23}	a_{31}	a_{32}	a_{33}
North limb	0.69	−0.25	0.68	−0.45	0.58	0.67	−0.57	−0.77	0.29
Hinge area	0.99	0.08	0.11	−0.13	0.78	0.60	−0.04	−0.62	0.78
South limb	0.88	−0.06	−0.47	0.05	0.99	−0.04	0.47	0.01	0.88

Table 4. Components of the mean March stretch tensors for the three sections of the fold (see text)

	s_{11}	s_{12}	s_{13}	s_{22}	s_{23}	s_{33}
North limb S_1	0.98	−0.12	−0.07	0.97	−0.04	1.06
Hinge area S_2	1.15	−0.02	0.01	1.01	−0.16	0.88
South limb S_3	1.05	0.01	0.18	1.12	−0.03	0.88

Table 5. Mean calculated principal tectonic stretches and their directions in the north limb, hinge area, south limb and overall, with a standard deviation of 0.01. t_1—maximum, t_2—intermediate, t_3—least

	t_1	Trend (°)	Plunge (°)	t_2	Trend (°)	Plunge (°)	t_3	Trend (°)	Plunge (°)
North limb	1.93	65	88	0.77	222	2	0.67	312	1
Hinge area	1.98	35	87	0.72	231	3	0.70	140	1
South limb	2.09	294	88	0.71	41	1	0.68	131	2
Overall	2.00	18	89	0.73	225	1	0.68	135	1

Table 6. Components of rotation matrices, separated from the transformation matrices $[T_iR_i]$ calculated from equations (4), with rotation angles of 0.99° for the north limb, 1.13° for the hinge area and 0.77° for the south limb

	r_{11}	r_{12}	r_{13}	r_{21}	r_{22}	r_{23}	r_{31}	r_{32}	r_{33}
North limb	1.00	0.00	−0.01	0.00	1.00	−0.02	0.01	0.02	1.00
Hinge area	1.01	0.01	−0.02	−0.01	0.99	−0.01	0.02	0.01	1.00
South limb	1.00	0.00	0.00	0.00	1.00	0.01	0.00	0.00	1.00

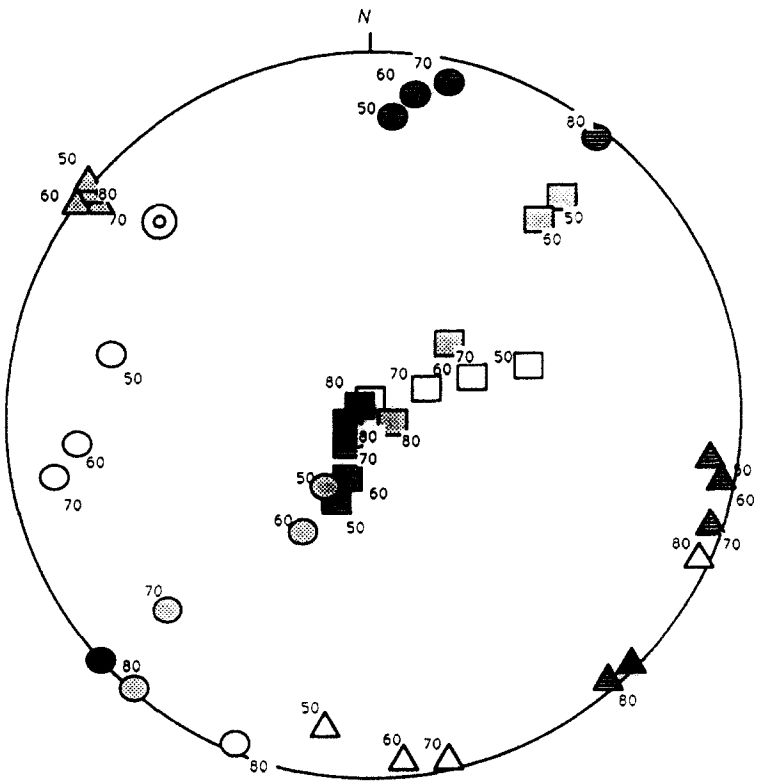

Fig. 10. Variation diagram of principal directions (equal-area projection) of the calculated tectonic stretches in the three sections of the fold, with changing pre-tectonic porosity, of 50, 60, 70 and 80%. Black—most probable principal directions in the three sections of the fold, at assumed pre-tectonic porosity of 79%. Other symbols are same as in Fig. 8.

shortening axes are approximately normal (intermediate) and parallel (least) to the fold axis.

DISCUSSION

Several questions remain to be answered. (1) What was the timing of the tectonic event or series of events? (2) How many separate episodes could possibly have been involved in the tectonic straining? (3) How was the folding history of the Los Prietos syncline related to the evolution of the pull-apart Santa Maria basin? (4) And what were the nature of the deformation and the rheology of the rocks during the deformation? Combined with additional field studies, the model of strain history here proposed could either provide constraints or some provisional answers to these questions.

The most probable porosity (79%) of the rocks before the onset of the tectonic event implies a depth of burial between 100 and 200 m (Fig. 2). This estimate allows one to time the event approximately, if the sediment accumulated at a known rate. Pisciotto & Garrison (1981) showed that 1 m of their third-order cyclical alternations of massive and laminated Monterey diatomites in the Lompoc area represents a time span of up to 1800 years. Therefore, the tectonic event should have begun between 0.18 and 0.36 Ma after the sediments were deposited. On the geologic time scale, the event was penecontemporaneous with deposition.

The mechanical nature of the deformation in the Los Prietos syncline is reflected only in its style. There is no direct quantitative method to study its paleo-rheology. However, by qualitative comparison with laboratory and mathematical model simulations (Biot 1957, Dieterich 1970, Johnson & Page 1976), the rocks appear to have acted as viscous multi-layers with a high viscosity contrast, so as to form tight small-scale kinkfolds. Intraformational structures, like those described in this paper, are commonly observed throughout the Monterey Formation. Although, these structures were previously described as soft-sediment deformation structures (Bramlette 1946, Redwine 1981, Snyder 1987), in the Los Prietos syncline, the axial attitudes of microfolds are parallel to those of the regional structures, and the microfolds were probably caused by the regional tectonic events. Considering that the tectonic movement may have been penecontemporaneous with deposition and that the resulting intraformational structures resemble soft-sediment structures due to gravitational slope failure, we conclude that tectonic movement tilted the basin floor and produced a tectonically controlled slope. Gravity then acted on unconsolidated Monterey sediments and made them creep down the tilting slope. The microfolds were thus given soft-sediment deformational features, but their axial attitudes coincide with the orientation of regional structures.

Because of lack of constraints, the tectonic history was here differentiated into no more than two distinct episodes, buckling and homogeneous strain. However, if a localized NNE–SSW basin stretching had occurred after the sediments were deposited, a corresponding stretching increment should be separable from the total finite homogeneous tectonic strain. Similarly, if a later NW–SE shortening had occurred during northwestward tilting, a consequence of the uplifting of the eastern part of the basin (indicated by Hall 1981), there should be a separate shortening increment ascribable to that event. That there were two increments seems plausible, based on the relationship between the geometry of the syncline and the orientations of the two principal shortening axes of the calculated total homogeneous tectonic stretch tensor (Fig. 10). Maximum shortening, instead of being normal to the syncline axis, is approximately parallel to the fold axis. The elongation due to continuing localized basin stretching possibly compensated for the maximum shortening normal to the fold axis. Such an explanation fits with a continuous history of basin opening. Moreover, the NW–SE shortening corresponding to the uplift of the eastern basin may also have exceeded the effect of elongation along the fold axis during folding; the cumulative strain along the fold axis therefore became a shortening rather than a stretching. However, as long as no physical markers for the different strain increments can be found, a strain history such as that described here must be regarded as mainly speculative.

A summary of what we regard as the most plausible strain history for the study area is as follows: between 12 and 14 Ma, contemporaneous with the Miocene transgression and as part of the evolution of the Miocene southern Californian continental borderland, the Santa Maria marine basin was extended and the Upper Monterey Formation was deposited. The original sediment porosity was gradually and incompletely reduced by the weight of the sediment overburden. Later, the still unconsolidated sediment flowed down a tilting slope caused by depression of the basin northeast of the study area and its later closing in the NE–SW direction. At this stage, the extensional, contractional and mixed features developed that resemble slope failure structures. Somewhere between 0.18 and 0.36 Ma after deposition, the major tectonic episode that could be related to the main basin compression affected the rocks at the stratigraphic level of the study area and buckled them to form the Los Prietos syncline. The uplifting of the eastern basin followed; it caused the syncline to plunge to the northwest and shortened the rocks along the fold axis. Thereafter, the sediments were further compacted and consolidated by the weight of the accumulated and tectonically thickened overburden.

CONCLUSIONS

This study of aspects of the strain history of the Monterey rocks in the Los Prietos syncline leads to the following tentative conclusions.

(1) The rocks at the studied stratigraphic level were deposited with an original pore-volume of 86%.

(2) Compaction by sediment overburden reduced porosity to 79%.

(3) Before any tectonic deformation, and at the shallow burial depth of 100–200 m, the various sediment layers had attained somewhat different degrees of cohesion, but all were still unconsolidated.

(4) The local slope failure triggered by uneven depression or uplift of the basement caused the unconsolidated sediment to be deformed. Extensional, contractional and mixed-origin features developed.

(5) The tectonic style of deformation is, therefore, that of a ductile material.

(6) The finite homogeneous tectonic stretches are, on the average [2.00, 0.73, 0.68], with a nominal standard deviation of 0.01. The tectonic strain leaves the volume unchanged, the axis of maximum stretching is nearly vertical, the axis of intermediate strain is horizontal and nearly normal to the fold axis, and the axis of least strain is horizontal and has the same trend as the fold axis.

(7) The homogeneous tectonic strain may be the cumulative effect of three increments, corresponding to the episodes of basin opening, folding and westward tilting. These increments, however, cannot be quantitatively separated.

(8) A large part of the total compaction followed the tectonic episode and further reduced the porosity from 79% to about 40–25%.

Acknowledgements—This study originated as a graduate thesis by R. T. Chen under the supervision of G. Oertel. We would like to thank A. G. Sylvester and W. L. Bartlett for their helpful field discussion, Bartlett for her suggestion of the fold profile and R. Alkaly for preparing thin sections for the X-ray goniometer. We are also grateful to J. M. Christie and W. E. Reed for their insightful reviews of an earlier version of this manuscript and greatly indebted for constructive criticism by P. J. Hudleston, C. K. Mawer and an anonymous reviewer. This research was partially supported by a gift from Texaco, Inc.

REFERENCES

Baker, D. W., Wenk, H.-R. & Christie, J. M. 1969. X-ray analysis of preferred orientation in fine-grained quartz aggregates. *J. Geol.* **77**, 144–172.

Biot, M. A. 1957. Folding instability of a layered viscoelastic medium under compression. *Proc. R. Soc. Lond.* **A242**, 444–454.

Blatt, H., Middleton, G. & Murray, R. 1980. *Origin of Sedimentary Rocks*. Prentice-Hall, Englewood Cliffs, New Jersey.

Bramlette, M. N. 1946. The Monterey Formation of California and the origin of its siliceous rocks. *Prof. Pap. U.S. geol. Surv.* **212**.

Brueckner, H. K., Snyder, W. S. & Boudreau, M. 1987. Diagenetic controls on the structural evolution of siliceous sediments in the Golconda allochthon, Nevada, U.S.A. *J. Struct. Geol.* **9**, 403–417.

Chen, R. T. 1986. Strain analysis of Monterey Formation rocks in the Los Prietos syncline, Santa Maria Basin, California. Unpublished M.S. thesis, University of California at Los Angeles.

Crowell, J. C. 1974. Origin of the Cenozoic basin in southern California. In: *Tectonics and Sedimentation* (edited by Dickinson, W. R.). *Spec. Publs Soc. econ. Paleont. Miner.* **22**, 190–204.

Dibblee, T. W., Jr. 1966. Geology of the Central Santa Ynez Mountains, Santa Barbara County, California. *Bull Calif. Div. Mines Geol.* **186**.

Dieterich, J. H. 1970. Computer experiments on mechanics of finite amplitude folds. *Can. J. Earth Sci.* **7**, 467–476.

Elliott, C. G. & Williams, P. F. 1988. Sediment slump structures: a review of diagnostic criteria and application to an example from Newfoundland. *J. Struct. Geol.* **10**, 171–182.

Etheridge, M. A. & Oertel, G. 1979. Strain measurements from phyllosilicate preferred orientation—a precautionary note. *Tectonophysics* **60**, 107–120.

Faas, R. W. & Crocket, D. S. 1983. Clay fabric development in a deep-sea core: Site 515, Deep Sea Drilling Project Leg 72. *Init. Rep. D.S.D.P.* **72**, 519–525.

Hall, C. A., Jr. 1978. Origin and development of the Lompoc–Santa Maria pull-apart basin and its relation to the San Simeon-Hosgri strike-slip fault, Western California. In: *San Gregorio–Hosgri Fault Zone, California* (edited by Silver, E. A. & Normark, W. R.). *Spec. Rep. Calif. Div. Mines Geol.* **137**, 25–31.

Hall, C. A., Jr. 1981. Evolution of the Western Transverse Ranges Micro-plate: late Cenozoic faulting and basinal development. In: *The Geotectonic Development of California* (edited by Ernst, W. G.). Prentice-Hall, Englewood Cliffs, New Jersey, 559–582.

Hamilton, E. L. 1976. Variations of Density and porosity with depth in deep sea sediments. *J. sedim. Petrol.* **46**, 280–300.

Hornafius, J. S. 1985. Neogene tectonic rotation of the Santa Ynez Range, western Transverse Ranges, California, suggested by paleomagnetic investigation of the Monterey Formation. *J. geophys. Res.* **90**, 12, 503–12, 522.

Hornafius, J. S., Luyendyk, B. P., Terres, R. R. & Kamerling, M. J. 1986. Timing and extent of Neogene tectonic rotation in the western Transverse Ranges, California. *Bull. geol Soc. Am.* **97**, 1476–1487.

Ingle, J. C., Jr. 1980. Cenozoic paleobathymetry and depositional history of selected sequence within the Southern California Continental Borderlands. In: *Studies in Micropaleontology* (edited by Sliter, W. V.). *Spec. Publ. Cushman Foundation for Foraminiferal Research* **19**, 163–195.

Isaacs, C. M. 1981. Guide to the Monterey Formation in the California Coastal Area, Ventura to San Luis Obispo. *Spec. Publs Am. Ass. Petrol. Geol. Pacific Sec.* 52.

Isaacs, C. M., Pisciotto, K. A. & Garrison, R. E. 1983. Facies and diagenesis of the Miocene Monterey Formation, California: A summary. In: *Developments in Sedimentology*, Volume 36 (edited by Iijima, A., Hein, J. R. & Siever, R.). Elsevier, Amsterdam, 247–282.

Johnson, A. M. & Page, B. M. 1976. A theory of concentric, kink and sinusoidal folding and of monoclinal flexuring of compressible, elastic multilayers. VII Development of folds within Huasna Syncline, San Luis Obispo County, California. *Tectonophysics* **33**, 97–143.

Krishnan, T. K. & Oertel, G. 1980. Aspects of strain history in folded sediments from the Schefferville mining district, Labrador Trough, Canada. *Tectonophysics* **64**, 33–46.

Luyendyk, B. P., Kamerling, M. J. & Terres, R. 1980. Geometric model for Neogene crustal rotations in southern California. *Bull. geol. Soc. Am.* **91**, 211–217.

Luyendyk, B. P. & Hornafius, J. S. 1987. Neogene crustal rotations, fault slip, and basin development in southern California. In: *Cenozoic Basin Development of Coastal California* (edited by Ingersoll, R. V. & Ernst, W. G.). Prentice-Hall, Englewood Cliffs, New Jersey, 259–283.

Maltman, A. 1984. On the term 'soft-sediment deformation'. *J. Struct. Geol.* **6**, 589–592.

March, A. 1932. Mathematische theorie der regelung nach der korngestalt bei affiner deformation. *Z. Kristallogr.* **81**, 285–297.

Meade, R. H. 1966. Factors influencing the early stages of the compaction of clays and sands: review. *J. sedim. Petrol.* **36**, 1085–1101.

Means, W. D. & Paterson, M. S. 1966. Experiments on preferred orientation of platy minerals. *Contr. Miner. Petrol.* **1**, 108–133.

Murata, K. J. & Larson, R. R. 1975. Diagenesis of Miocene siliceous shales, Temblor Range, California. *J. Res. U.S. Geol. Surv.* **3**, 553–566.

Moon, C. F. & Hurst, C. W. 1984. Fabric of muds and shales: an overview. In: *Fine-Grained Sediments: Deep-Water Processes and Facies* (edited by Stow, D. A. V. & Piper, D. J. W.). *Spec. Publs geol. Soc. Lond.* **15**, 579–594.

Oertel, G. 1970. Deformation of slaty lapillar tuff in the Lake District, England. *Bull. geol. Soc. Am.* **81**, 1173–1188.

Oertel, G. 1974. Unfolding of an antiform by the reversal of observed strains. *Bull. geol. Soc. Am.* **85**, 445–450.

Oertel, G. 1983. The relationship of strain and preferred orientation of phyllosilicate grains in rocks: a review. *Tectonophysics* **100**, 413–447.

Oertel, G. & Curtis, C. D. 1972. Clay-ironstone concretion preserving fabrics due to progressive compaction. *Bull. geol. Soc. Am.* **83**, 2597–2606.

Oertel, G. & Ernst, W. G. 1978. Strain and rotation in a multilayered fold. *Tectonophysics* **48**, 77–106.

Pisciotto, K. A. & Garrison, R. E. 1981. Lithofacies and depositional environments of the Monterey Formation, California. In: *The*

Monterey Formation and Related Siliceous Rocks of California (edited by Garrison, R. E. & Douglass, R. G.). *Spec. Publs Soc. econ. Paleont. Miner. Pacific Sec.* **15**, 87–95.

Redwine, L. 1981. Hypothesis combining dilation, natural hydraulic-fracturing, and dolomitization to explain petroleum reservoirs in Monterey Shales, Santa Maria area, California. In: *The Monterey Formation and Related Siliceous Rocks of California* (edited by Garrison, R. E. & Douglass, R. G.). *Spec. Publs Soc. econ. Paleont. Miner. Pacific Sec.* **15**, 221–248.

Roehl, R. O. 1981. Dilation brecciation—A proposed mechanism of fracturing, petroleum expulsion and dolomitization in the Monterey Formation, California. In: *The Monterey Formation and Related Siliceous Rocks of California* (edited by Garrison, R. E. & Douglass, R. G.). *Spec. Publs Soc. econ. Paleont. Miner. Pacific Sec.* **15**, 285–316.

Snyder, W. S. 1987. Structure of the Monterey Formation: stratigraphic, diagenetic and tectonic influences on style and timing. In: *Cenozoic Basin Development of Coastal California* (edited by Ingersoll, R. V. & Ernst, W. G.). Prentice-Hall, Englewood Cliffs, New Jersey, 321–347.

Snyder, W. S., Brueckner, H. K. & Schweickert, R. A. 1983. Deformation styles in the Monterey Formation and other siliceous sedimentary rocks. In: *Petroleum Generation and Occurrence in the Miocene Monterey Formation, California* (edited by Isaacs, C. M. & Garrison, R. E.). *Spec. Publs Soc. econ. Paleont. Miner. Pacific Sec.* **15**, 151–170.

Tullis, T. E. 1971. Experimental development of preferred orientation of mica during recrystallization. Unpublished thesis, University of California, Los Angeles; University Microfilms, Ann Arbor, Michigan.

Tullis, T. E. 1976. Experiments on the origin of slaty cleavage and schistosity. *Bull. geol. Soc. Am.* **87**, 745–753.

Tullis, T. E. & Wood, D. S. 1975. Correlation of finite strain from both reduction bodies and preferred orientation of mica in slate from Wales. *Bull. geol. Soc. Am.* **86**, 632–638.

Wood, D. S., Oertel, G., Singh, J. & Bennett, H. F. 1976. Strain and anisotropy in rocks. *Phil. Trans. R. Soc. Lond.* **A283**, 27–42.

Wenk, H.-R. 1985. Measurement of pole figures. In: *Preferred Orientation in Deformed Metals and Rocks: An Introduction to Modern Texture Analysis* (edited by Wenk, H.-R.). Academic Press, Orlando, 11–47.

Woodring, W. P. & Bramlette, M. N. 1950. Geology and paleontology of the Santa Maria district, California. *Prof. Pap. U.S. geol. Surv.* **222**.